mater.scichina.com link.springer.com

Published online 17 May 2024 | https://doi.org/10.1007/s40843-024-2956-9
*Sci China Mater* 2024, 67(6): 1882–1890

SPECIAL TOPIC: Advanced Energy Catalytic Materials

# Stabilization of MOF-derived $Co_3S_4$ nanoparticles *via* graphdiyne coating for efficient oxygen evolution

Mengyu Lu[†], Xin Zhao[†], Shifu Zhang, Hengxin Jian, Mei Wang[*] and Tongbu Lu[*]

**ABSTRACT** **Developing a facile approach to fabricate robust electrocatalysts for the oxygen evolution reaction (OER) is essential for water electrolysis for hydrogen production. Transition metal-organic frameworks (MOFs), with their diverse coordination geometries, offer a promising avenue for deriving materials with excellent electrocatalytic properties. Leveraging the distinct controllable synthesis features of two-dimension graphdiyne (2D-GDY), we herein present a novel strategy: Loading GDY *in situ* onto a MOF-derived $Co_3S_4$/nickel foam (NF) material to create a self-supported electrode, GDY/$Co_3S_4$/NF, exhibiting significantly enhanced electrocatalytic performances for OER. Our comprehensive investigation reveals that GDY/$Co_3S_4$/NF demonstrates superior performance, with a low overpotential of 223 mV at a current density of 10 mA cm$^{-2}$ and a small Tafel slope of 46.5 mV dec$^{-1}$. Notably, it showcases exceptional stability over 45 h of continuous electrolysis at a high current density of 100 mA cm$^{-2}$ under alkaline conditions, highlighting its promising practical applicability. These results validate that the unique acetylene bonds and macroporous structure of 2D-GDY enable strong electronic interactions with $Co_3S_4$, thereby tuning the electronic configuration, facilitating efficient charge transport channels, increasing active surface areas, and enhancing durability. Furthermore, *in-situ* attenuated total reflection surface-enhanced infrared spectroscopy (*in-situ* ATR-SEIRAS) analysis reveals that the synergistic effect between GDY and $Co_3S_4$ promotes the adsorption of crucial intermediate species such as OOH$^*$, thereby significantly improving the electrocatalytic activity for OER. This work presents a facile and efficient strategy for constructing advanced nanomaterials with extraordinary electrocatalytic performance, offering promising prospects for various practical applications.**

**Keywords:** GDY, cobalt-based sulfides, MOF-derived $Co_3S_4$, electrocatalysis, OER

## INTRODUCTION

Amidst the escalating challenges posed by energy crises and environmental degradation, there is a pressing need for concerted efforts towards the development of cleaner and sustainable energy alternatives to supersede traditional fossil fuels [1–3]. Hydrogen, renowned for its high energy density and zero carbon emissions, emerges as a promising candidate for various crucial applications in the quest for sustainable energy solutions [4]. Electrocatalytic water splitting, powered by renewable energy sources, is widely considered as the most promising method for scalable hydrogen production [5–7]. However, the sluggish reaction kinetics and high thermodynamic potentials of the oxygen evolution reaction (OER), which serve as the half-reaction in water splitting, significantly hinder the efficiency of hydrogen production. To date, noble-metal oxides, particularly RuO and IrO, are widely acknowledged as the most efficient electrocatalysts for OER [8–10]. Nevertheless, their high cost, scarcity, and poor stability have posed significant obstacles to their practical applications. Therefore, the quest for efficient, robust, and economical electrocatalysts for OER has become a compelling and critical research pursuit [11].

In recent years, substantial efforts have been directed towards the rational exploration of non-precious transition metal-based electrocatalysts through the manipulation of electronic configurations for OER. Specifically, integrating cobalt ions with unfilled d orbitals in the valence layer and sulfide elements with lower electronegativity has the potential to significantly tune the electronic structure of the catalyst, thereby enhancing its catalytic reactivity towards OER [12–15]. However, the precise engineering of the electronic and geometric structures of cobalt-based sulfide catalysts to achieve optimal performance for OER remains a significant challenge.

Metal-organic frameworks (MOFs) have shown immense promises in the design of cutting-edge catalysts for OER, owing to their tailored compositions, intricate structures, and adjustable pore sizes [16–18]. However, several limitations such as poor stability under harsh electrochemical conditions and low conductivity hinder their widespread practical use. To address these issues, researchers have devised various strategies to develop MOF-derived materials with exceptional properties, opening new avenues for the efficient development of OER electrocatalysts [19,20]. For instance, various earth-abundant transition metal phosphide like CoP [21], transition metal oxides like $CoFe_2O_4$ [22], and transition metal chalcogenides like $Fe_2$ NiSe [23] derived from MOF precursors, have demonstrated high catalytic reactivity for OER. Among these derivatives,

School of Materials Science and Engineering, Tianjin University of Technology, Tianjin 300384, China
[†] These authors contributed equally to this work.
[*] Corresponding authors (emails: meiwang@email.tjut.edu.cn (Wang M); lutongbu@tjut.edu.cn (Lu T))

  

cobalt-based sulfides derived from MOFs have garnered significant attention due to their tunable structure, abundant active sites, enhanced electrical conductivity, and efficient mass transfer properties, all contributing to their outstanding performances in electrocatalytic OER. To further boost the OER performances of cobalt-based sulfides, numerous strategies have been implemented to optimize their electronic structure, ranging from coatings, metal doping, to loading onto supports [24–27]. Despite these advancements, cobalt-based sulfides still encounter challenges in electrocatalytic OER, including relatively low long-term stability, sluggish charge transfer rates, and high overpotentials. Addressing these challenges remains a crucial task in order to fully harness the potential of cobalt-based sulfides for efficient OER.

Utilizing carbon-based nanomaterials in tandem with transition metal electrocatalysts to optimize interfacial interactions has proven to be an innovative approach for enhancing catalytic performance of OER [28–30]. Among these carbon-based materials, graphdiyne (GDY), a novel all-carbon allotrope, stands out. It possesses a unique 2D honeycomb lattice structure comprising alternating triple and single bonds between sp- and $sp^2$-hybridized carbon atoms [31,32]. This unique –C≡C–C≡C– arrangement offers exceptional properties such as high electrical conductivity, tunable active sites, chemical stability, vast surface area, and sustainability. These remarkable properties have led to significant advancements in various research areas, particularly in energy storage and electrocatalysis [33–37]. Specifically, the unique –C≡C–C≡C– structure of GDY enables effective interactions with transition metal nanomaterials through a strong metal-support interaction (SMSI) effect. This interaction significantly enhances charge transfer between GDY and transition metal centers, optimizing the electronic configuration of the catalysts and stabilizing them [37–40]. Furthermore, GDY exhibits remarkable stability in both acidic and alkaline environments, providing exceptional protection for catalysts and ensuring robust catalytic durability [41–45]. Unlike other carbon materials, GDY can be synthesized through a cross-coupling reaction under mild conditions, facilitating its coating onto diverse nanomaterials to enhance their catalytic properties [46–48]. For instance, Li *et al.* [49] developed an efficient OER electrocatalyst, NW-MnCoO/GDY, by layering GDY onto MnCoO nanowires through an *in-situ* growth strategy. This work demonstrates the synergistic interaction between MnCoO and GDY, which significantly improves the catalytic performance of the electrocatalyst for OER. Moreover, our design of ultra-small quasi-core/shell RuO-Ru nanoparticles, when loaded onto GDY, yielded an outstanding catalyst, RuO-Ru/GDY, for the OER. This remarkable performance is attributed to the precise regulation of the electron density of Ru in the RuO shell by the unique interaction with GDY [50]. These advancements illustrate that, decorating transition metal nanomaterials with GDY to finely tune their electronic structures, presents significant opportunities for enhancing their electrocatalytic performances in the OER.

In this study, we introduce a pioneering approach, pioneering the creation of an advanced OER catalyst by decorating cobalt sulfides derived from MOFs with GDY. We utilize nickel foam (NF) as the foundation, directly growing cobalt-based MOFs, ZIF-67, onto its surface. Subsequently, through sulfurization, we achieve a uniform distribution of blade-shaped $Co_3S_4$/NF. Next, we coat GDY onto the surface of $Co_3S_4$ *via* an *in-situ* growth technique, yielding GDY/$Co_3S_4$/NF, which exhibits remarkably improved electrocatalytic performance for OER. The self-supported electrode, GDY/$Co_3S_4$/NF, demonstrates outstanding characteristics, including a low overpotential of 223 mV at a current density of 10 mA $cm^{-2}$, a minimal Tafel slope of 46.5 mV $dec^{-1}$, and stable electrolysis for over 45 h at a significant current density of 100 mA $cm^{-2}$ under alkaline conditions. This underscores its significant potential for industrial applications. *In-situ* attenuated total reflection surface-enhanced infrared spectroscopy (*in-situ* ATR-SEIRAS) analysis reveals that the modification of $Co_3S_4$/NF with GDY enhances the adsorption of the crucial intermediate $OOH^*$, thereby bolstering its catalytic properties. Our findings confirm that the exceptional electrocatalytic performance primarily stems from the SMSI effect between GDY and $Co_3S_4$, profoundly modulating its electronic properties, thus optimizing charge transfer and increasing active sites during the catalytic process. Furthermore, the exceptional chemical and physical properties of GDY significantly bolster the stability of our designed GDY/$Co_3S_4$/NF catalyst for OER.

## EXPERIMENTAL SECTION

### Synthesis of ZIF-67/NF

ZIF-67/NF was synthesized using an *in-situ* growth approach. Initially, NF pieces (1 × 2 $cm^2$) were cleaned by sonication in 3 M hydrochloric acid for 10 min to eliminate the oxide layer from the surface. Subsequently, they were rinsed sequentially with deionized water, ethanol, and acetone, followed by vacuum drying. Next, the dried NFs were vertically immersed in a prepared mixed solution containing 0.58 g of $Co(NO_3)_2{\cdot}6H_2O$ and 1.313 g of 2-methylimidazole dissolved in deionized water. After 48 h of undisturbed reaction, ZIF-67 grew directly on the NF, resulting in ZIF-67/NF. The resulting material was washed with water, ethanol, and acetone successively, followed by vacuum drying at 50°C for 2 h.

### Synthesis of $Co_3S_4$/NF

$Co_3S_4$/NF was synthesized using a simple sulfurization method. Initially, 0.25 g of thioacetamide was dissolved in 35 mL of ethanol. Subsequently, a piece of ZIF-67/NF obtained from the previous steps was immersed in the solution, which was then transferred to a hydrothermal reactor and heated to 130°C for 12 h in an oven. After the system was cooled to room temperature, the resulting $Co_3S_4$/NF material was washed with water and ethanol several times, followed by vacuum drying at 60°C for several hours.

### Synthesis of GDY/$Co_3S_4$/NF

The precursor of GDY, hexaethynylbenzene (HEB), was synthesized under an argon atmosphere following previously reported traditional methods [33,51]. Subsequently, the obtained $Co_3S_4$/NF was placed inside a rounded copper foil, which was then immersed in a mixed solution containing 5 mL of pyridine, 100 mL of acetone, and 1 mL of tetramethylethylenediamine (TMEDA). HEB dissolved in a 50 mL acetone solution was then added dropwise to the above system. The mixture was heated at 55°C for 12 h to obtain GDY/$Co_3S_4$/NF, which was rinsed with deionized water, ethanol, and acetone, and then dried in a vacuum at 60°C for 8 h.

## RESULTS AND DISCUSSION

### Synthesis and characterization of the GDY/$Co_3S_4$/NF electrocatalysts

As outlined in Scheme 1, the fabrication of the self-supported electrode GDY/$Co_3S_4$/NF comprises three pivotal steps. Initially, through a refined process, ZIF-67 is directly deposited onto NF to obtain the precursor ZIF-67/NF, by precisely controlling the ratio of $Co^{2+}$ ions and 2-methylimidazole ligands at ambient temperature [52]. Subsequently, the ZIF-67/NF is transformed into $Co_3S_4$/NF *via* a conventional hydrothermal route using thioacetamide as the sulfur source [53,54]. Lastly, GDY is synthesized *in-situ* through a coupling reaction, effectively coating the surface of $Co_3S_4$, ultimately yielding the final product, GDY/$Co_3S_4$/NF.

The surface morphologies of various samples, including ZIF-67/NF, $Co_3S_4$/NF, and GDY/$Co_3S_4$/NF, were thoroughly characterized using scanning electron microscopy (SEM) (Fig. 1a and Fig. S1). SEM analysis reveals that ZIF-67 exhibits a distinct three-dimensional (3D) leaf-like morphology, which undergoes significant alterations after undergoing high-temperature carbonization and etching, resulting in a noticeably roughened surface (Fig. 1b). Upon the *in-situ* growth of GDY nanowalls onto the surface of $Co_3S_4$, forming GDY/$Co_3S_4$/NF, the original structure of $Co_3S_4$ is beautifully preserved. However, a new layer of wrinkle-like GDY nanowall emerges on the surface (Fig. 1c, d), significantly enhancing the roughness compared with both ZIF-67/NF and $Co_3S_4$/NF. This observation provides a compelling evidence of the successful and uniform coating of GDY onto $Co_3S_4$/NF, which is crucial for its outstanding electrocatalytic performance towards OER. High-resolution transmission electron microscopy (HRTEM) analysis further delves into the morphological nuances of GDY/$Co_3S_4$/NF. As depicted in Fig. 2b, distinct lattice fringes with a d-spacing of 0.238 nm are observed, corresponding to the (311) facet of $Co_3S_4$. Additionally, the selected area electron diffraction (SAED) pattern (inset in Fig. 2a) exhibits a series of diffraction rings with bright spots, indicative of the polycrystalline nature of the catalyst. Furthermore, energy dispersive X-ray spectroscopy (EDS) mapping images (Fig. 2d–h) reveal the uniform distributions of

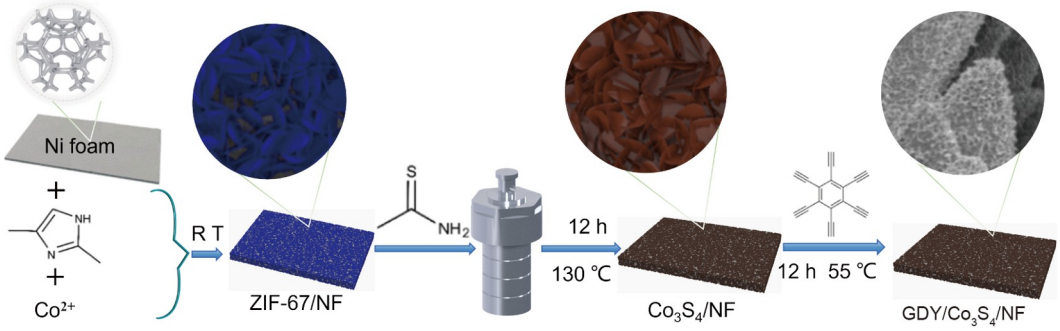


**Scheme 1** The synthesis process of the material.

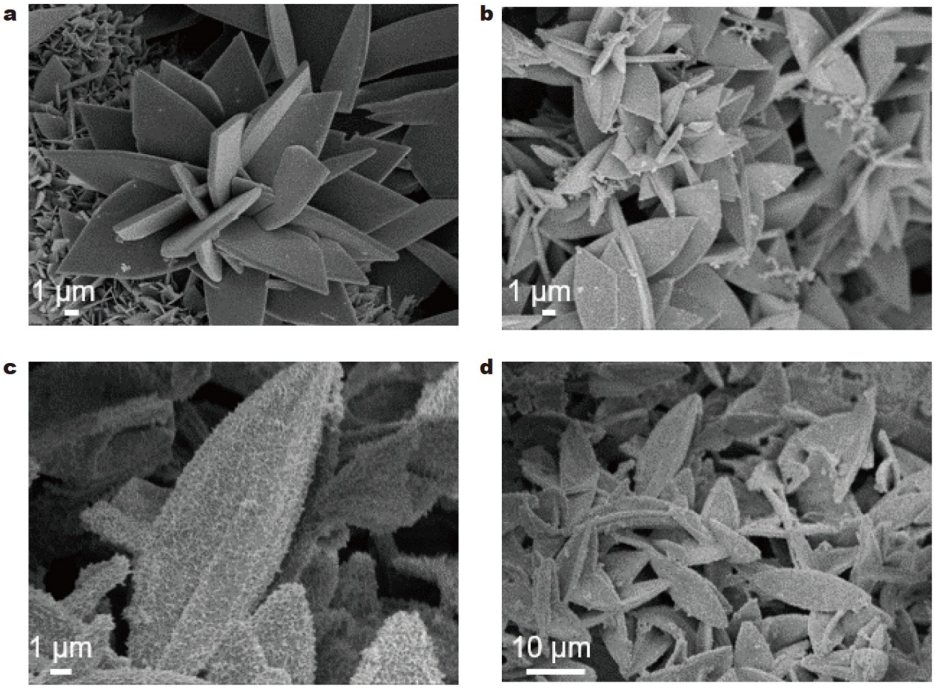


**Figure 1** SEM images of (a) ZIF-67/NF, (b) $Co_3S_4$/NF, (c, d) GDY/$Co_3S_4$/NF.

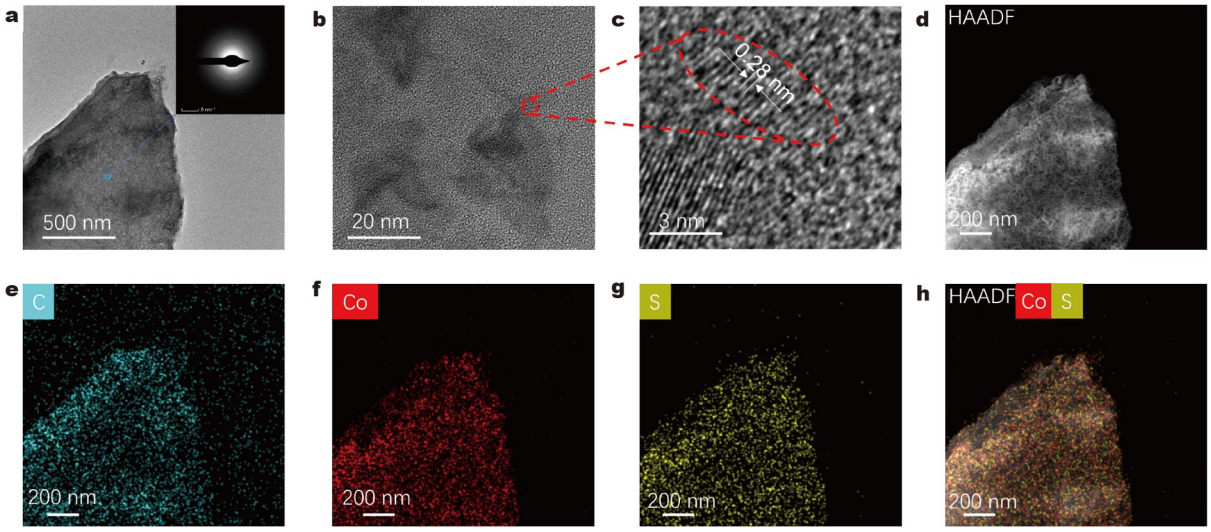


**Figure 2** (a) TEM images of GDY/$Co_3S_4$/NF, the inset is SAED pattern. (b, c) HRTEM images of GDY/$Co_3S_4$/NF. (d–h) EDS elemental mapping images of GDY/$Co_3S_4$/NF.

Co, S, and C elements within the GDY/$Co_3S_4$ composite, thus confirming the robust integration of GDY and $Co_3S_4$. Powder X-ray diffraction analysis (PXRD) is also performed to elucidate the structural characteristics of the synthesized samples (Fig. 3a). Notably, all samples exhibit three prominent peaks at 44.5°, 51.8° and 76.4°, corresponding to the (111), (200) and (220) planes of NF (JCPDS NO. 87-0712), respectively. In the case of ZIF-67/NF, the ZIF-67 peaks are faintly observable due to the overlapping diffraction peaks with NF. However, after the sulfidation process, both $Co_3S_4$/NF and GDY/$Co_3S_4$/NF exhibit distinct characteristic peaks at 31.5°, 38.2°, 50.4° and 55.2°, corresponding to the (311), (400), (511) and (440) crystal planes of $Co_3S_4$ (JCPDS NO. 73-1703), respectively, thereby affirming the successful synthesis of the target materials.

Raman spectroscopy is utilized to gain further insights into the chemical composition and structural features of the prepared samples. As depicted in Fig. 3b (bottom), the Raman shifts at 293, 498 and 641 $cm^{-1}$ are ascribed to $Co_3S_4$ [55]. Meanwhile, for the GDY/$Co_3S_4$/NF composite (Fig. 3b, top), peaks at 293, 323 and 393 $cm^{-1}$ in the low-frequency region correspond to $Co_3S_4$. In the high-frequency region, peaks centered at 1376 and 1586 $cm^{-1}$ are associated with the breathing vibration (D band) and in-phase stretching vibration (G band) of $sp^2$-hybridized carbons in the benzene rings of GDY, respectively. Additionally, peaks located at 1933 and 2174 $cm^{-1}$ are attributed to the vibrational modes of conjugated diyne groups (–C≡C–C≡C–) within the GDY structure of GDY/$Co_3S_4$/NF. These comprehensive findings provide unequivocal evidences for the successful synthesis of our designed self-supported electrode, GDY/$Co_3S_4$/NF. Furthermore, X-ray photoelectron spectroscopy (XPS) analyses are conducted to probe the chemical states and composition of the synthesized materials (Fig. 3c–f and Fig. S2). The comprehensive XPS spectra at the top of Fig. 3c clearly exhibit the presence of Co, S, and C elements in the GDY/$Co_3S_4$/NF composite, which aligns well with the findings from EDS. The oxygen detected is likely due to atmospheric exposure. Specifically, the Co 2p spectrum in Fig. 3d reveals characteristic peaks of Co $2p_{3/2}$ and Co $2p_{1/2}$ centered at 781.0 and 796.0 eV, respectively, accompanied by satellite peaks. These main peaks can be further decomposed into two groups, namely 778.9 and 780.2 eV for $Co^{3+}$ and 793.9 and 795.7 eV for $Co^{2+}$, confirming the coexistence of cobalt ions in two distinct valence states [56]. Additionally, a slight shift in the binding energy of the main peaks when comparing GDY and Co indicates a robust electronic interaction between GDY and $Co_3S_4$, thus validating the successful coating of GDY on $Co_3S_4$/NF. In the high-resolution S 2p spectra depicted in Fig. 3e, peaks centered around 162.3 and 164.1 eV correspond to S $2p_{3/2}$ and S $2p_{1/2}$, respectively, representing the Co–S bond in $Co_3S_4$. The peak at 169.7 eV likely originates from sulfur oxides resulting from surface sulfur oxidation upon air exposure [57]. For the C 1s XPS spectrum of GDY/$Co_3S_4$/NF (Fig. 3f), four deconvoluted peaks are observed, corresponding to $sp^2$-hybridized C=C (284.3 eV), sp-hybridized C≡C (285.1 eV), C–O (286.6 eV), and C=O (288.9 eV), respectively. These XPS results provide further confirmation of the successful synthesis of the GDY/$Co_3S_4$/NF composite. When compared with pure GDY, the GDY/$Co_3S_4$/NF composite exhibits a slight shift in the binding energies of the four characteristic C 1s peaks. This observation signifies the existence of a robust electronic interaction between GDY and $Co_3S_4$, thereby validating the successful integration of GDY onto the $Co_3S_4$/NF catalyst. This interaction is particularly beneficial for enhancing the electrocatalytic OER, indicating that the GDY/$Co_3S_4$/NF composite is a promising candidate for promoting efficient electrocatalysis.

### Electrocatalytic OER performance

The electrocatalytic performances of the synthesized samples towards water oxidation are rigorously evaluated in a standard three-electrode cell under alkaline conditions (1 M KOH) at a scan rate of 5 mV $s^{-1}$. All reported potentials are referenced to the reversible hydrogen electrode (RHE). The working electrodes consist of our self-supported GDY/$Co_3S_4$/NF electrode, alongside two comparative samples: $Co_3S_4$/NF and ZIF-67/NF. The counter electrode is a carbon rod, and the reference electrode is Hg/HgO. The polarization curves and subsequent analyses in Fig. 4a, b reveal that GDY/$Co_3S_4$/NF exhibites remarkable electrocatalytic activities, achieving overpotentials of just 223 and 407 mV at current densities of 10 and 100 mA $cm^{-2}$, respectively. These values are significantly lower

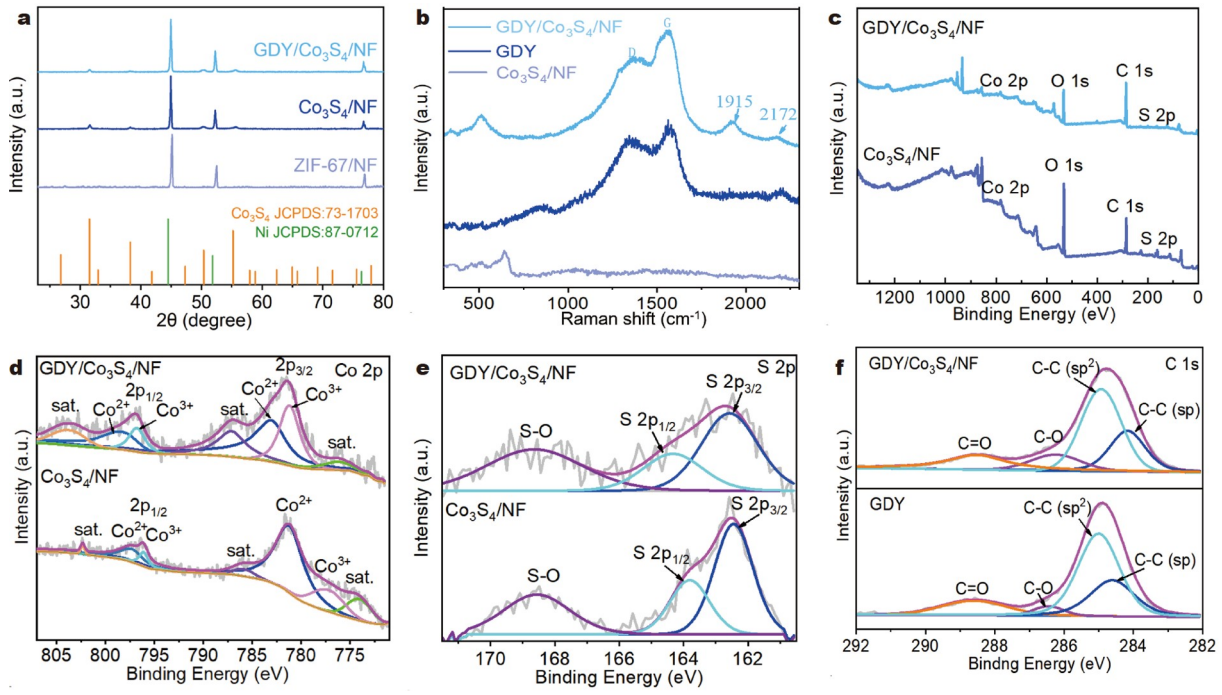


**Figure 3** (a) XRD patterns of $Co_3S_4$/NF and GDY/$Co_3S_4$/NF. (b) Raman spectra of $Co_3S_4$/NF and GDY/$Co_3S_4$/NF. (c) XPS spectra of $Co_3S_4$/NF and GDY/$Co_3S_4$/NF. (d) Co 2p XPS spectra of $Co_3S_4$ and GDY/$Co_3S_4$/NF. (e) S 2p XPS spectra of $Co_3S_4$/NF and GDY/$Co_3S_4$/NF. (f) C 1s XPS spectra of GDY and GDY/$Co_3S_4$/NF.

than those observed for $Co_3S_4$/NF (230 and 463 mV) and ZIF-67/NF (359 and 529 mV), and they outperform numerous previously reported electrocatalysts (Table S1 and Fig. 4f). These findings underscore the superior OER performance of GDY/$Co_3S_4$/NF compared with the other catalysts [13,26,27,58–60]. To further elucidate the reaction kinetics of the electrocatalytic OER, Tafel slope analyses and electrochemical impedance spectroscopy (EIS) are performed. As shown in Fig. 4c, GDY/$Co_3S_4$/NF exhibits a substantially lower Tafel slope of 46.5 mV $dec^{-1}$ compared with $Co_3S_4$/NF (78.9 mV $dec^{-1}$) and ZIF-67/NF (132.9 mV $dec^{-1}$). It indicates that our GDY/$Co_3S_4$/NF electrode possesses higher conductivity and faster reaction kinetics during the electrocatalytic $O_2$ evolution reaction. Additionally, the EIS Nyquist plots (Fig. 4d) demonstrate that the GDY/$Co_3S_4$/NF electrode exhibits the smallest semicircle diameter among the three samples, suggesting enhanced charge transfer efficiency between the electrode and the electrolyte interface during the OER process. Moreover, to quantify the electrochemical active surface area (ECSA), double-layer capacitance ($C_{dl}$) is evaluated through cyclic voltammetry (CV) measurements conducted at varying scan rates from 10 to 100 mV $s^{-1}$ within the non-Faradaic voltage window of 0.6–0.7 V *vs.* RHE (Fig. S3). Linear regression analysis of the scan rate and the corresponding current density derived from the CV data (Fig. 4e) reveal that GDY/$Co_3S_4$/NF possesses the highest $C_{dl}$ of 6.09 mF $cm^{-2}$, surpassing $Co_3S_4$/NF (4.28 mF $cm^{-2}$) and ZIF-67/NF (3.28 mF $cm^{-2}$). This substantial increase in $C_{dl}$ suggests a notable expansion of the active surface area achieved by coating porous GDY onto $Co_3S_4$/NF. These collective findings convincingly demonstrate that the integration of GDY onto $Co_3S_4$/NF significantly optimizes the intrinsic properties of the catalyst, leading to enhanced OER performance. The enhancement is primarily attributed to the robust electronic interaction between GDY and $Co_3S_4$, which facilitates the regulation of the catalyst's electronic structure and geometry.

Furthermore, to evaluate the practical applicability of the catalyst, its long-term stability is assessed through chronopotentiometry measurements. As illustrated in Fig. 4g, GDY/$Co_3S_4$/NF demonstrates exceptional stability, maintaining a constant potential for over 45 h at a high and consistent current density of 100 mA $cm^{-2}$ during the OER. This remarkable stability outperforms numerous recently reported catalytic materials, with $Co_3S_4$/NF, for instance, exhibiting stability for only 17.5 h [13,61]. To gain further insights into the microscopic morphology and chemical composition of the catalyst after prolonged OER testing, we conduct SEM, XRD, and XPS analyses (Figs S4–S6). The SEM images reveal that the morphology of GDY/$Co_3S_4$/NF remains well-preserved even after the extended catalysis period (Fig. S4). Moreover, the XRD and XPS measurements conducted post-electrocatalysis for OER are in alignment with the pre-catalysis results (Figs S5, S6), further affirming the exceptional stability of our designed OER electrocatalyst, GDY/$Co_3S_4$/NF. This stability can be attributed to the acid- and alkali-resistant, corrosion-resistant GDY nanomaterial coating outside $Co_3S_4$, which effectively stabilizes the electrocatalyst.

To gain a deeper understanding of the catalytic mechanism of GDY/$Co_3S_4$/NF for OER, we conduct *in-situ* ATR-SEIRAS experiments (Fig. S7). These measurements are performed at varying potentials ranging from 1.25 to 1.70 V *vs.* RHE in a 1 M KOH solution to identify the intermediates involved in the electrocatalytic OER process. As shown in Fig. 5, at the open circuit potential (OCP), neither GDY/$Co_3S_4$/NF nor $Co_3S_4$/NF exhibits any prominent peaks. However, for GDY/$Co_3S_4$/NF (Fig. 5 right), a distinct peak at 1013 $cm^{-1}$ is observed, which exhibits an increasing trend as the potential increases from 1.25

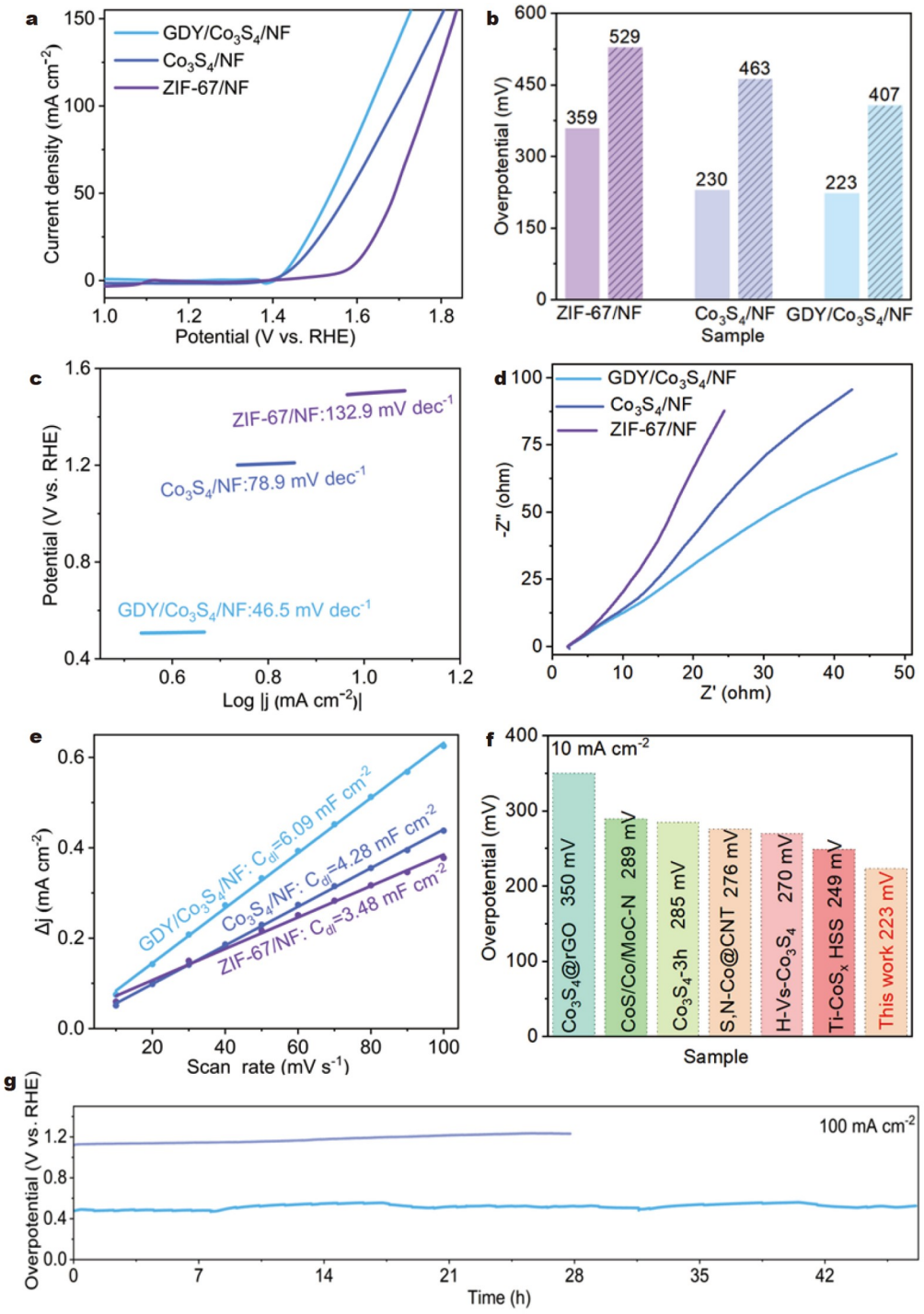


**Figure 4** (a) LSV diagrams of ZIF-67/NF, $Co_3S_4$/NF and GDY/$Co_3S_4$/NF. (b) Overpotential bar diagrams of three materials, left 10 mA cm$^{-2}$, right 100 mA cm$^{-2}$. (c) Tafel of three materials. (d) EIS maps of three materials. (e) $C_{dl}$ diagrams of three materials. (f) Comparison of overpotential of GDY/$Co_3S_4$/NF with similar catalysts at a current density of 10 mA cm$^{-2}$. (g) Constant current stability tests of GDY/$Co_3S_4$/NF and $Co_3S_4$/NF.

to 1.70 V. This peak is attributed to the stretching vibration of the OOH$^*$ species [62–65], indicating its formation and accumulation during the OER process. Under alkaline conditions, the OER catalyzed by GDY/$Co_3S_4$/NF likely follows the traditional adsorbate evolution mechanism (AEM). This mechanism involves the rate-determining step of O–O bond formation through the nucleophilic attack of $OH^-$ to produce the key intermediate OOH$^*$, followed by the desorption of oxygen through the deprotonation of OOH$^*$ [66,67]. In contrast, for $Co_3S_4$/NF (Fig. 5 left), a potential-dependent peak at 1019 cm$^{-1}$ corresponding to the OOH$^*$ species is observed, albeit at a higher energy level compared to GDY/$Co_3S_4$/NF. This suggests that the key intermediate OOH$^*$ is adsorbed more strongly on the active sites of GDY/$Co_3S_4$/NF than on $Co_3S_4$/NF. It results in a lower free energy of OOH$^*$ adsorption on GDY/$Co_3S_4$/NF, leading to significantly higher catalytic reactivity. The observed differences

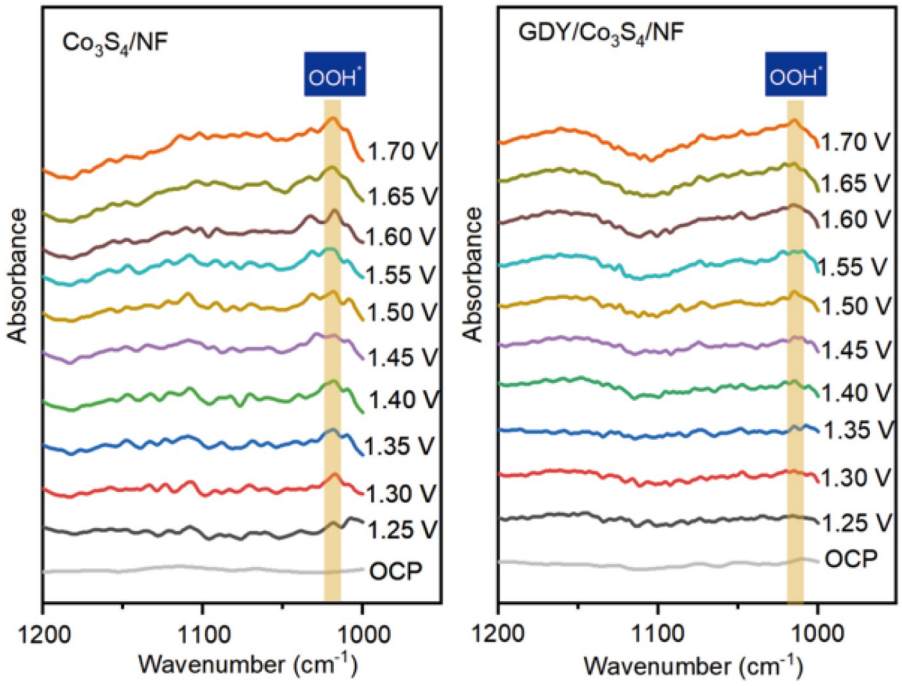


**Figure 5** Comparison of *in situ* ATR-SEIRAS measurements at different potentials of $Co_3S_4$/NF (left) and GDY/$Co_3S_4$/NF (right).

in $OOH^*$ adsorption can be attributed to the unique interaction between the acetylene carbon in GDY and the Co metal centers in $Co_3S_4$. This SMSI effect facilitates charge transfer between GDY and $Co_3S_4$, optimizing the electronic configuration of the catalyst and facilitating the binding of the crucial intermediate $OOH^*$ with a lower energy. Consequently, GDY/$Co_3S_4$/NF exhibits superior OER performance compared with $Co_3S_4$/NF. The insights gained from the *in-situ* ATR-SEIRAS measurements underscore the superiority of the GDY-decorated $Co_3S_4$/NF catalyst for electrocatalytic oxygen evolution compared to $Co_3S_4$/NF. These findings align perfectly with the previously mentioned results of the electrocatalytic performance tests, further validating the enhanced reactivity exhibited by the GDY/$Co_3S_4$/NF composite. Specifically, the unique interaction between the acetylene carbon in GDY and the Co metal centers in $Co_3S_4$ results in a stronger adsorption of the crucial $OOH^*$ intermediate on the active sites of GDY/$Co_3S_4$/NF, leading to a lower free energy of adsorption and thus significantly higher catalytic reactivity for oxygen evolution.

## CONCLUSIONS

In summary, we have developed an innovative method for the precise fabrication of an advanced self-supported electrode for OER through the *in-situ* deposition of 2D-GDY onto MOF-derived CoS/NF. The resulting GDY/CoS/NF catalyst exhibits a distinct 3D morphology and exceptional catalytic performance for water oxidation. Specifically, it achieves a remarkable low overpotential of 223 mV at a current density of 10 mA $cm^{-2}$ and a small Tafel slope of 46.5 mV $dec^{-1}$. Impressively, it sustains stable electrolysis for over 45 h, even at a high current density of 100 mA $cm^{-2}$, under alkaline conditions. Our in-depth *in-situ* ATR-SEIRAS spectroscopic analysis reveals that the integration of GDY onto CoS/NF significantly enhances the adsorption of the crucial intermediate $OOH^*$, leading to improved catalytic properties.

The introduction of GDY to CoS promotes strong interactions with cobalt ions through its alkynyl carbon, which modulates the electronic configuration and increases the number of active sites, thereby bolstering the electrocatalytic OER performance. Moreover, the incorporation of porous 2D-GDY optimizes the structure, greatly facilitating mass and charge transfer. Furthermore, the remarkable chemical stability of GDY ensures enhanced durability of the catalyst when coated onto CoS. This study underscores the powerful potential of decorating MOF-derived transition metal nanomaterials with GDY as a promising approach for developing highly effective and stable catalysts.

**Received 30 March 2024; accepted 26 April 2024; published online 17 May 2024**

1 Kwak WJ, Rosy WJ, Sharon D, *et al.* Lithium-oxygen batteries and related systems: potential, status, and future. Chem Rev, 2020, 120: 6626–6683
2 Jaramillo TF, Jørgensen KP, Bonde J, *et al.* Identification of active edge sites for electrochemical $H_2$ evolution from $MoS_2$ nanocatalysts. Science, 2007, 317: 100–102
3 Chulliyote R, Hareendrakrishnakumar H, Raja M, *et al.* Sulfur-immobilized nitrogen and oxygen co-doped hierarchically porous biomass carbon for lithium-sulfur batteries: Influence of sulfur content and distribution on its performance. Chem Select, 2017, 2: 10484–10495
4 Anantharaj S, Noda S, Jothi VR, *et al.* Strategies and perspectives to catch the missing pieces in energy-efficient hydrogen evolution reaction in alkaline media. Angew Chem Int Ed, 2021, 60: 18981–19006
5 Wang J, Zhang Z, Ding J, *et al.* Recent progresses of micro-nanostructured transition metal compound-based electrocatalysts for energy conversion technologies. Sci China Mater, 2021, 64: 1–26
6 Yang Y, Zhang K, Lin H, *et al.* $MoS_2$-$Ni_3S_2$ heteronanorods as efficient and stable bifunctional electrocatalysts for overall water splitting. ACS Catal, 2017, 7: 2357–2366
7 Kibsgaard J, Chorkendorff I. Considerations for the scaling-up of water splitting catalysts. Nat Energy, 2019, 4: 430–433

  

8 Ouyang T, Wang X, Mai X, *et al.* Coupling magnetic single-crystal $Co_2Mo_3O_8$ with ultrathin nitrogen-rich carbon layer for oxygen evolution reaction. Angew Chem Int Ed, 2020, 59: 11948–11957
9 Yang D, Chen D, Jiang Y, *et al.* Carbon-based materials for all-solid-state zinc-air batteries. Carbon Energy, 2020, 3: 50–65
10 Liu Q, Xie L, Qu F, *et al.* A porous $Ni_3N$ nanosheet array as a high-performance non-noble-metal catalyst for urea-assisted electrochemical hydrogen production. Inorg Chem Front, 2017, 4: 1120–1124
11 Shi Q, Zhu C, Du D, *et al.* Robust noble metal-based electrocatalysts for oxygen evolution reaction. Chem Soc Rev, 2019, 48: 3181–3192
12 Shahzad A, Zulfiqar F, Arif Nadeem M. Cobalt containing bimetallic ZIFs and their derivatives as OER electrocatalysts: A critical review. Coord Chem Rev, 2023, 477: 214925
13 Sahu N, Behera JN. MOF-derived $Co_3S_4$ nanoparticles embedded in nitrogen-doped carbon for electrochemical oxygen production. ACS Appl Nano Mater, 2023, 6: 7686–7693
14 Lamiel C, Hussain I, Rabiee H, *et al.* Metal-organic framework-derived transition metal chalcogenides (S, Se, and Te): Challenges, recent progress, and future directions in electrochemical energy storage and conversion systems. Coord Chem Rev, 2023, 480: 215030
15 Li S, Gao Y, Li N, *et al.* Transition metal-based bimetallic MOFs and MOF-derived catalysts for electrochemical oxygen evolution reaction. Energy Environ Sci, 2021, 14: 1897–1927
16 Qin X, Kim D, Piao Y. Metal-organic frameworks-derived novel nanostructured electrocatalysts for oxygen evolution reaction. Carbon Energy, 2021, 3: 66–100
17 Xue X, Gao H, Liu J, *et al.* Electrostatic potential-derived charge: A universal OER performance descriptor for MOFs. Chem Sci, 2022, 13: 13160–13171
18 Wang T, Gao L, Hou J, *et al.* Rational approach to guest confinement inside MOF cavities for low-temperature catalysis. Nat Commun, 2019, 10: 1–9
19 Yang D, Chen Y, Su Z, *et al.* Organic carboxylate-based MOFs and derivatives for electrocatalytic water oxidation. Coord Chem Rev, 2021, 428: 213619
20 Li Z, Song M, Zhu W, *et al.* MOF-derived hollow heterostructures for advanced electrocatalysis. Coord Chem Rev, 2021, 439: 213946
21 Zong H, Qi R, Yu K, *et al.* Ultrathin $Ti_2NT_x$ MXene-wrapped MOF-derived CoP frameworks towards hydrogen evolution and water oxidation. Electrochim Acta, 2021, 393: 139068
22 Fu Y, Wang W, Wang J, *et al.* MOFs-derived ZnCo-Fe core-shell nanocages with remarkable oxygen evolution reaction performance. J Mater Chem A, 2019, 7: 17299–17305
23 Guo Y, Zhang C, Zhang J, *et al.* Metal-organic framework-derived bimetallic NiFe selenide electrocatalysts with multiple phases for efficient oxygen evolution reaction. ACS Sustain Chem Eng, 2021, 9: 2047–2056
24 Xu H, Cao J, Shan C, *et al.* MOF-derived hollow CoS decorated with $CeO_x$ nanoparticles for boosting oxygen evolution reaction electrocatalysis. Angew Chem Int Ed, 2018, 57: 8654–8658
25 Nguyen AN, Tran NM, Yoo H. Direct growth and post-treatment of zeolitic imidazolate framework-67 on carbon paper: An effective and stable electrode system for electrocatalytic reactions. J Mater Chem A, 2022, 10: 20770–20778
26 Bao T, Xia Y, Lu J, *et al.* A pacman-like titanium-doped cobalt sulfide hollow superstructure for electrocatalytic oxygen evolution. Small, 2022, 18: 2103106
27 Santhosh Kumar R, Karthikeyan SC, Ramakrishnan S, *et al.* Anion dependency of spinel type cobalt catalysts for efficient overall water splitting in an acid medium. Chem Eng J, 2023, 451: 138471
28 Jiang X, Xie Q, Lu G, *et al.* Synthesis of $NiSe_2/Fe_3O_4$ nanotubes with heteroepitaxy configuration as a high-efficient oxygen evolution electrocatalyst. Small Methods, 2022, 6: 2200377
29 Lin YH, Zhang Q, Ding SC, *et al.* NiFe nanoparticle nest supported on graphene as electrocatalyst for highly efficient oxygen evolution reaction. Small, 2023, 20: 2308278
30 Lin L, Wang Y, Ye Q, *et al.* Rapid fabrication of $FexNi_2$-$xP_4O_{12}$ and graphene hybrids as electrocatalyst for highly efficient oxygen evolution reaction. Appl Catal B-Environ, 2023, 334: 122834
31 Chen X, Zheng X, Zhang C, *et al.* Highly selective conversion of $CO_2$ to formate on SnOx/GDY heterostructured electrocatalyst. Nano Energy, 2023, 114: 108622
32 Wang M, Pu J, Hu Y, *et al.* Functional graphdiyne for emerging applications: Recent advances and future challenges. Adv Funct Mater, 2024, 34: 2308601
33 Li G, Li Y, Liu H, *et al.* Architecture of graphdiyne nanoscale films. Chem Commun, 2010, 46: 3256
34 Zuo Z, Wang D, Zhang J, *et al.* Synthesis and applications of graphdiyne-based metal-free catalysts. Adv Mater, 2019, 31: 1803762
35 Gao X, Liu H, Wang D, *et al.* Graphdiyne: synthesis, properties, and applications. Chem Soc Rev, 2019, 48: 908–936
36 Li M, Wang K, Lv Q. N,P-co-doped graphdiyne as efficient metal-free catalysts for oxygen reduction reaction. Chem Res Chin Univ, 2021, 37: 1283–1288
37 Xue Y, Huang B, Yi Y, *et al.* Anchoring zero valence single atoms of nickel and iron on graphdiyne for hydrogen evolution. Nat Commun, 2018, 9: 1460
38 Shi GD, Xie YL, Du LL, *et al.* Constructing Cu–C bonds in a graphdiyne-regulated Cu single-atom electrocatalyst for $CO_2$ reduction to $CH_4$. Angew Chem Int Ed, 2022, 61: e202203569
39 Fu X, Zhao X, Lu T, *et al.* Graphdiyne-based single-atom catalysts with different coordination environments. Angew Chem Int Ed, 2023, 62: e202219242
40 Gao Y, Cai Z, Wu X, *et al.* Graphdiyne-supported single-atom-sized fe catalysts for the oxygen reduction reaction: DFT predictions and experimental validations. ACS Catal, 2018, 8: 10364–10374
41 Wang S, Che Z, Zou M, *et al.* Gorgeous turn-back: Rough surface treatment strategy induces Cu-C and N-C active moieties for bifunctional oxygen electrocatalysis. Chem Eng J, 2023, 471: 144262
42 Chen B, Jiang YF, Xiao H, *et al.* Bimetallic single-cluster catalysts anchored on graphdiyne for alkaline hydrogen evolution reaction. Chin J Catal, 2023, 50: 306–313
43 Wang Z, Zheng Z, Xue Y, *et al.* Acidic water oxidation on quantum dots of $IrO_x$/graphdiyne. Adv Energy Mater, 2021, 11: 2101138
44 Qi L, Chen Z, Luan X, *et al.* Atomically dispersed Mn enhanced catalytic performance for overall water splitting on graphdiyne-coated copper hydroxide nanowire. Chin J Struct Chem, 2024, 43: 100197
45 Liu Y, Xue Y, Yu H, *et al.* Graphdiyne ultrathin nanosheets for efficient water splitting. Adv Funct Mater, 2021, 31: 2010112
46 Yu S, Chen J, Chen C, *et al.* What happens when graphdiyne encounters doping for electrochemical energy conversion and storage. Coord Chem Rev, 2023, 482: 215082
47 Qi L, Gao Y, Gao Y, *et al.* Controlled growth of metal atom arrays on graphdiyne for seawater oxidation. J Am Chem Soc, 2024, 146: 5669–5677
48 Zheng Z, Xue Y, Li Y. A new carbon allotrope: graphdiyne. Trends Chem, 2022, 4: 754–768
49 Qi L, Zheng Z, Xing C, *et al.* 1D nanowire heterojunction electrocatalysts of $MnCo_2O_4$/GDY for efficient overall water splitting. Adv Funct Mater, 2022, 32: 2107179
50 Chen X, Fu X, Zhang S, *et al.* Graphdiyne *in situ* thermal reduction enabled ultra-small quasi-core/shell Ru-$RuO_2$ heterostructures for efficient acidic water oxidation. 2D Mater, 2021, 8: 044011
51 Wang S, Yi L, Halpert JE, *et al.* A novel and highly efficient photocatalyst based on P25-graphdiyne nanocomposite. Small, 2012, 8: 265–271
52 Zhao XJ, Fang XL, Wu BH, *et al.* Facile synthesis of size-tunable ZIF-8 nanocrystals using reverse micelles as nanoreactors. Sci China Chem, 2014, 57: 141–146
53 Li G, Wang P, Li C, *et al.* Cobalt-nickel layered double hydroxide on hollow $Co_3S_4$/CuS derived from ZIF-67 for efficient overall water splitting. Mater Res Lett, 2022, 10: 744–753
54 Yang Y, Ma Q, Han L, *et al.* Zeolitic imidazolate framework-derived $Co_3S_4$@$Co(OH)_2$ nanoarrays as self-supported electrodes for asymmetric supercapacitors. Inorg Chem Front, 2019, 6: 1398–1404
55 Ji K, Che Q, Yue Y, *et al.* Ni-doped $Co_3S_4$ hollow nanobox for the hydrogen evolution reaction. ACS Appl Nano Mater, 2022, 5: 9901–9909
56 Lee YJ, Park S. Metal-organic framework-derived hollow $CoS_x$ na-


  

noarray coupled with NiFe layered double hydroxides as efficient bifunctional electrocatalyst for overall water splitting. Small, 2022, 18: 2200586
57 Guo Y, Tang J, Qian H, *et al.* One-pot synthesis of zeolitic imidazolate framework 67-derived hollow $Co_3S_4$@$MoS_2$ heterostructures as efficient bifunctional catalysts. Chem Mater, 2017, 29: 5566–5573
58 Ren Y, Wang H, Zhang T, *et al.* Designed preparation of CoS/Co/MoC nanoparticles incorporated in N and S dual-doped porous carbon nanofibers for high-performance Zn-air batteries. Chin Chem Lett, 2021, 32: 2243–2248
59 Rao P, Liu Y, Su YQ, *et al.* S, N co-doped carbon nanotube encased Co NPs as efficient bifunctional oxygen electrocatalysts for zinc-air batteries. Chem Eng J, 2021, 422: 130135
60 Li X, Zheng K, Zhang J, *et al.* Engineering sulfur vacancies in spinel-phase $Co_3S_4$ for effective electrocatalysis of the oxygen evolution reaction. ACS Omega, 2022, 7: 12430–12441
61 Li Z, Xu W, Yu X, *et al.* Synergistic effect between 1D $Co_3S_4$/$MoS_2$ heterostructures to boost the performance for alkaline overall water splitting. Inorg Chem Front, 2022, 9: 2139–2149
62 Liu H, Zhang Z, Fang J, *et al.* Eliminating over-oxidation of ruthenium oxides by niobium for highly stable electrocatalytic oxygen evolution in acidic media. Joule, 2023, 7: 558–573
63 Cheng W, Zhao X, Su H, *et al.* Lattice-strained metal-organic-framework arrays for bifunctional oxygen electrocatalysis. Nat Energy, 2019, 4: 115–122
64 Liu H, Qi Z, Song L. *In situ* electrocatalytic infrared spectroscopy for dynamic reactions. J Phys Chem C, 2021, 125: 24289–24300
65 Kumar G, Haldar R, Shanmugam M, *et al.* Mechanistic insight into a Co-based metal-organic framework as an efficient oxygen electrocatalyst *via* an *in situ* FT-IR study. J Mater Chem A, 2023, 11: 26508–26518
66 Xin S, Tang Y, Jia B, *et al.* Coupling adsorbed evolution and lattice oxygen mechanism in Fe-$Co(OH)_2$/$Fe_2O_3$ heterostructure for enhanced electrochemical water oxidation. Adv Funct Mater, 2023, 33: 2305243
67 Li X, Deng C, Kong Y, *et al.* Unlocking the transition of electrochemical water oxidation mechanism induced by heteroatom doping. Angew Chem Int Ed, 2023, 62: e202309732

**Acknowledgements** This work was supported by the National Natural Science Foundation of China (22375148) and the National Key R&D Program of China (2022YFA1502902).

**Author contributions** Lu M and Zhang S designed and engineered the samples; Lu M, Zhao X and Zhang S performed the experiments; Jian H did some analyses. Wang M and Lu M wrote the paper with support from Lu T. Lu T and Wang M administrated the project, supervised the experiments and reviewed the manuscript. All authors contributed to the general discussion.

**Conflict of interest** The authors declare that they have no conflict of interest.

**Supplementary information** Experimental details and supporting data are available in the online version of the paper.

**Mengyu Lu** is a graduate student at the School of Materials Science and Engineering, Tianjin University of Technology. She received her BE degree from the Jiangxi University of Science and Technology in 2022. She is mainly engaged in the application of metal-based nanomaterials in electrocatalysis.

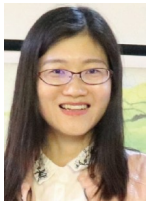

**Mei Wang** received her PhD degree in 2009 at the Fujian Institute of Research on the Structure of Matter, Chinese Academy of Sciences. Then she worked as a postdoctoral fellow at Max-Planck Institute for Chemical Energy Conversion. She is currently an associate professor at Tianjin University of Technology, working on metalbased complexes and nanomaterials synthesis, and exploring their applications in electrocatalysis.

**Tongbu Lu** obtained his BS in 1988 and PhD in 1993 from Lanzhou University. He joined the Sun Yat-Sen University and became a professor in 2000. In 2016, he moved to Tianjin University of Technology. His current research interest focuses on the study of artificial photosynthesis, including the design of homogeneous and heterogeneous catalysts for water splitting and $CO_2$ reduction. He obtained the National Natural Science Foundation for Distinguished Youth Scholar in 2006.

## 石墨炔涂层稳定MOF衍生物$Co_3S_4$纳米材料用于高效电催化析氧反应

陆梦玉[†], 赵欣[†], 张士福, 寥恒欣, 王梅[*], 鲁统部[*]

**摘要** 制备高效的OER电催化剂对水裂解制氢至关重要. 具有丰富配位构型的MOFs可以衍生出各种优良的电催化材料. 由于石墨炔(GDY)具有独特的可控合成特性, 我们将其原位复合在MOF衍生的$Co_3S_4$/NF材料上, 获得了自支撑电极GDY/$Co_3S_4$/NF, 大大提高了其OER催化性能. 研究表明, GDY/$Co_3S_4$/NF在10 mA $cm^{-2}$电流密度下表现出223 mV的低过电位, 在100 mA $cm^{-2}$的大电流密度下, 能够稳定电解45小时左右, 该材料显示出了巨大的实际应用潜力. 结果表明, 由于GDY独特的炔键和大孔结构, 它可以通过强电子相互作用与$Co_3S_4$相互作用, 从而调节电子结构并提供有效的电荷转移通道, 从而大大提高了其电催化OER的性能.

  